Field-induced conformational changes in bimetallic oligoaniline junctions

Juan C. Sotelo,[1] Liuming Yan, Michael Wang,[1] and Jorge M. Seminario[1,2]
[1]*Department of Chemical Engineering, Texas A&M University, College Station, Texas 77843, USA*
[2]*Department of Electrical and Computer Engineering, Texas A&M University, College Station, Texas 77843, USA*
(Received 26 August 2006; revised manuscript received 23 October 2006; published 21 February 2007)

We report three types of nonplanar conformations, α, β, and γ, for a neutral isolated oligoaniline molecule as well as for an oligoaniline with Au and Pd atoms attached at its ends. Each type of conformation has several conformers of nearly equal energies. An applied external voltage can be used to switch between conformations, producing in the process a sharp decrease of their energies. These bias voltage-induced conformational changes are a potential switching mechanism for two terminal molecular devices at the nanoscale domain. They cause the conductivity of the molecule to alternate between high and low states, compensating for the behavior of typical three-terminal devices, needed for the development of a gate-less electronics.

DOI: 10.1103/PhysRevA.75.022511 PACS number(s): 31.15.Ew, 33.15.Bh, 31.70.Ks, 31.15.Ar

I. INTRODUCTION

Molecular switches are essential components in molecular electronics devices as they constitute the building blocks in logic architectures. Lately, much effort has been devoted to the identification of these switches, and to the understanding of the intrinsic mechanisms governing their switching properties. Many types of switching mechanisms have been identified, among them, photon-induced [1], change of redox state [2–4], and electrically induced switching [5–8] to name a few. A typical electrically driven molecular switch consists of a single molecule, or many of them, e.g., self-assembled monolayer (SAM), adsorbed on metal electrodes, which can be electrically toggled between a high conductance (ON) state and a low conductance (OFF) state, with the ON and OFF states being stable enough for a large number of switching cycles. Recently, it has been shown experimentally that for a wide range of temperatures oligoaniline molecular junctions can exhibit electrical bistability and switch between a high and low conducting states in response to an applied external bias voltage [7]. It was suggested this behavior might be due to a redistribution of charges in the molecule coupled with a shift in molecular conformations [7].

In this paper we show that there are three main types of conformations for the standalone and for the extended (with electrode atoms of Au or Pd) oligoaniline molecule, called α, β, and γ, which undergo conformational changes under the influence of an external longitudinal electric field. In an Au-oligoaniline-Pd junction, when equilibrium is reached at room temperature, α has the highest probability to be present in the junction, β has the smallest. Furthermore, when the junction is subjected to an external bias voltage there is an interconversion between the α and γ conformations leading to a switching behavior between high γ and low α current states in the junction, as observed in experiments [7].

We deal with the conformational changes by considering first an extended oligoaniline molecule as a protojunction where a sought after property of a molecular switch, such as conformational changes, can be probed more easily [9,10]. Although by considering just the extended molecule, the interaction with the leads of both the extending metal atoms and the molecule is missing, and the dielectric effect of the leads on the field is not considered, nevertheless, it can still help elucidate the field-induced changes in molecular conformation and electronic structure for the following reasons. First, on a first approximation the interaction metal-molecule may be considered local, with metal atoms in direct contact with the molecule or in the near neighborhood contributing the most. This is, in fact, just a restatement of the rationale behind treating a molecular junction as a metal-extended-molecule-metal system [11–14]. Second, the molecular and electronic structures of the extended molecule are those obtained directly from *ab initio* calculations, which should allow for a detailed analysis at the atomic level of structural (e.g., bond length, torsional angles) and electronic properties (e.g., polarization, charge distribution) changes taken place within a molecule exposed to an external field. Such a fine level of resolution is lost when bulk electrodes are brought into consideration because of the coarse approximations that have to be made to treat them in present electron transport models. Ultimately, to take full advantage of molecular devices one would like to interconnect them, at most, through small metal clusters rather than through bulk metal solids [8]. Once the key properties of the extended molecule have been established, they can be included within an appropriate framework, such as the Green function method introduced below, to study the current through the junction.

This paper is organized as follows. Section II introduces the computational methods for dealing with the electronic properties of finite clusters and bulk electrodes, and the current-voltage (I-V) characterization of the junctions. Section III presents the DOS and transmission spectra for all conformations, as well as their I-V characteristics at fixed geometries. The section ends with a discussion of conformational changes under applied electric fields. Finally, Sec. IV summarizes the results of this work.

II. METHODOLOGY AND PROCEDURE

Density functional theory (DFT) and Green's function (GF) theory are used to study the electrical properties of conformations of the standalone oligoaniline and oligoaniline junctions. Basically, three different types of calcula-

 ©2007 The American Physical Society

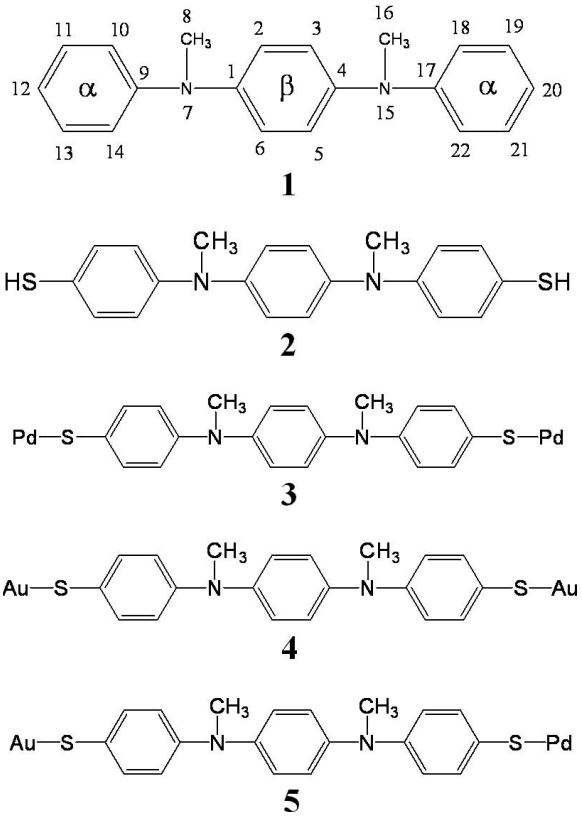

FIG. 1. **1** oligoaniline (N,N′-dimethyl-N,N′-diphenyl-1,4-benzenediamine), **2** oligoaniline with thiol groups used as clips attaching the molecule to Au or Pd electrodes, **3** oligoaniline with Pd contact atoms on each side, **4** oligoaniline with Au contact atoms on each side, **5** oligoaniline with Au and Pd contact atoms at left and right sides, respectively.

tions are carried out: the *ab initio* DFT calculations for the standalone and extended oligoaniline molecules (calculations for finite systems), the *ab initio* DFT calculation with periodic boundary conditions for the bulk materials (*ab initio* study of infinite electrodes), and the Green's function calculation for the electron transport through the junctions (DFT-GF approach).

A. *Ab initio* calculations for finite systems

The oligoaniline molecule **1** (Fig. 1) is composed of two amine groups and three benzene rings, its derivative, **2**, is self-assembled on Au or Pd surfaces forming a metal-*S*-oligoaniline-*S*-metal junctions, using Au or Pd electrodes (**3**, **4**, and **5**) in Fig. 1). Reversible bistable switching has been demonstrated in such molecular junctions, [7] with the bistable characteristics being attributed to possible molecular conformation changes occurring as the applied bias voltage across the junction reaches certain thresholds. In this work, the structure of these systems is studied in detail using *ab initio* quantum chemistry calculations, followed by the evaluation of electron transfer properties are using a Green's function approach based on the empirical Landauer theory [15–17].

The *ab initio* calculations are performed for the molecules (without the Au and Pd atoms) and for their extended versions (molecules where some contact atoms have been added) at the Becke three-parameter, Perdew-Wang 1991 (B3PW91) functional level of theory [18–21] as implemented in the GAUSSIAN 03 program [22] The correlation-consistent polarization valence triple zeta (cc-pVTZ) basis set is used for **1**. A combined basis set is implemented for the extended molecule **3**; the 6-31G is used for the C, H, N atoms and the Los Alamos effective core potential plus double zeta (LANL2DZ) for S, Au, Pd. For **5** and Au_2-**5**-Pd_2, we use the LANL2DZ. The use of different basis sets allows us to compare similar calculations we performed in the past with similar molecules. The use of the cc-pVTZ for **1** yields a high precision calculation as only first row atoms are involved. This basis set is not available for Au or Pd for instance. However, the difference between the 6-31G and the LANLDZ for C, H, and N is practically meaningless as both are double-ζ type basis sets. An extended molecule should not be confused in our nomenclature with an extended or periodic system such as a crystal of Au or Pd.

In order to find all the conformational isomers, the geometrical optimizations are run from several initial geometries for each system. All conformational isomers are verified to be local minima by the calculation of their Hessian matrix (or frequency calculation). Relative stabilities of the conformational isomers are compared on the basis of their corresponding total energies.

Perhaps, it is also important to clarify that although the precise shape of the contact may produce a strong impact in the I-V characteristics, our goal is to choose one shape of the contact and use it equally for several conformations with the minimum adaptations to get a stable contact-molecule pair so we can compare molecules attached to relatively similar contacts. In no way the goal is to determine what is the contact used experimentally as this also depends on the specific fabrication procedure and irreproducible conditions of experiments. So far, it is evident that there is not unique contact geometry for a single molecule. This is something that molecular electronics have to deal in the near future; new techniques and different scenarios need to be developed and tried in order to have a realistic implementation of the field [8,23].

B. *Ab Initio* study for extended systems

The DOS (density of states) of bulk or extended (periodic) systems of Au and Pd are calculated using the CRYSTAL 03 program [24,25]. For Pd, a hybrid density functional with LDA exchange [26] and Perdew-Zunger correlation [27] and a basis set of Stuttgart with relativistic small core ECP pseudopotentials [28–30] are used. For Au, the calculation is performed using the B3LYP functional [18] and LANL2DZ basis set and core potentials [30]. In both cases the experimental lattice parameters are used [31].

The Fermi energy obtained for Pd is −5.69 eV which is in good agreement with the experimental value of −5.60 eV [31]. The calculated Fermi energy of Au, on the other hand, is −5.80 eV, overestimated by about 10% compared to the experimental value of −5.31 eV [31]. From the projected DOS of Au and Pd (Fig. 2) it follows that the main contribution to the total DOS near the Fermi level arises from the *d* bands, d_{eg} and d_{t2g}, with d_{t2g} contributing the largest share.

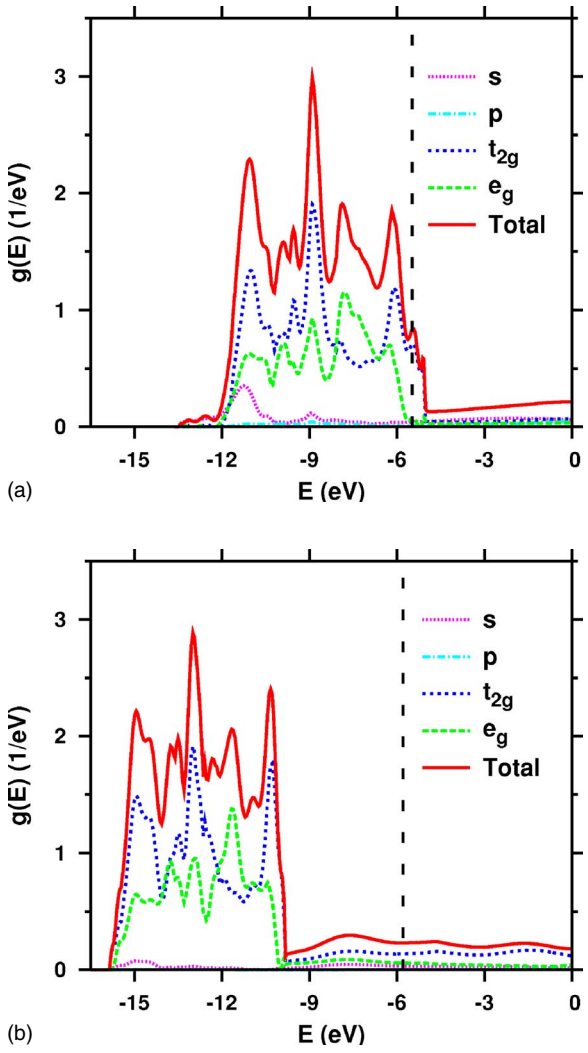

FIG. 2. (Color online) DOS of (a) palladium, solid (red), and (b) gold, solid (red). The DOS is projected onto the *s*, dotted (purple), *p*, dashed-dotted (light blue), d_{eg}, dashed (green) and d_{t2g}, long-dotted (blue), bands; these projections are helpful because the coupling between the electrodes and the molecule depends on the symmetry of the orbitals. The vertical dashed lines are drawn at the Fermi energy of the bulk metals.

Interestingly, Pt, the best catalyst, has the Fermi level at the starting of the *d* band as opposed to gold that have it at the tail.

C. The DFT-GF approach

The Green's function (GF) and density functional theory (DFT) are used to study the electrical characteristics of the bimetallic oligoaniline junctions, Pd_{bulk}-**3**-Pd_{bulk}, Au_{bulk}-**5**-Pd_{bulk}, and $Au_{bulk}Au_2$-**5**-Pd_2Pd_{bulk}. This notation [32] indicates that the standalone molecule, **1**, is extended with metal atoms on each side, in place of the end H atoms, as follows: in the first case, one Pd-atom at each end, yielding molecule **3**; in the second, one Au atom on the left and one Pd atom on the right, yielding molecule **5** [Fig. 3(a)]; and in the last, three-Au atoms on the left and three-Pd atoms on the right, yielding molecule Au_2-**5**-Pd_2 [Fig. 3(b)]. In all cases, the

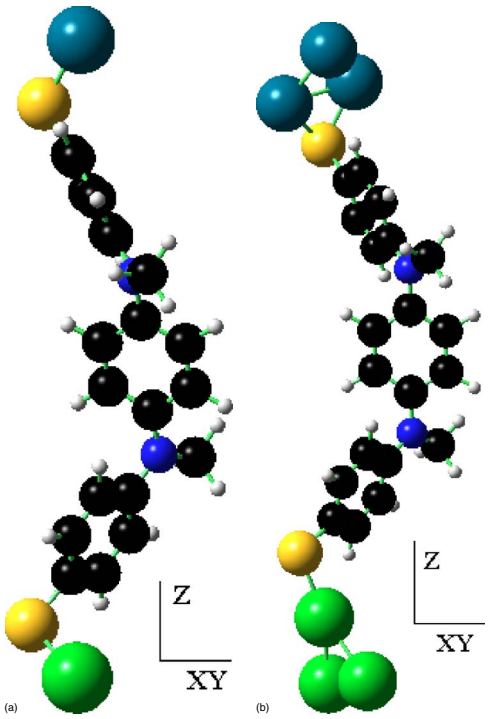

FIG. 3. (Color online) Extended molecules **5** (a) and Au_2-**5**-Pd_2 (b). Palladium atoms [top single (a) and top trimer (b)] are colored dark green; gold atoms [bottom single (a) and bottom trimer (b)] light green. The other atoms are colored as follows: sulfur, interfacing the metal atoms with the rest of the molecule, yellow; nitrogen, joining the benzene rings, blue; carbon, black; and hydrogen, light gray. See also Fig. 1 for a chemical formula of **5**. The *z* axis in the figure defines the direction of the applied electric field.

extended molecule is then attached at both ends to semi-infinite bulk leads of metals matching the extending atoms.

Our procedure is as follows, see also [8,32–34] and references therein: (1) The geometry of the extended molecule is optimized in the absence of field using the GAUSSIAN 03 program [22] until a local energy minimum is obtained. As varying the initial geometry usually leads to several local minima, several optimized geometries may result at this stage. (2) A frequency calculation is carried out on the optimized geometries to guarantee the stability of the extended molecule. (3) For each applied bias electric field at which the current is calculated, we either use a fixed optimized molecule geometry found in (2), or optimize the molecule geometry under field, and then proceed to compute the Hamiltonian and overlap matrices of the extended molecule at that particular field. Thus, every point of the *I-V* curve corresponds to a full *ab initio* calculation under field. (4) The DOS for the bulk materials is obtained using the CRYSTAL 03 program [35,36]. (5) Through a Green's function transport scheme explained below, the Hamiltonian and overlap matrices obtained in step three are combined with the bulk DOSs obtained in step four to yield the DOS, electron transmission probabilities and *I-V* characteristics of the molecule. In this procedure, the self-consistent treatment used when the bias electric field is applied to the extended molecule ensures that the chemistry of the molecule is not lost throughout the calculations.

In the GF method, the Green's function of the standalone molecule, G_M, is obtained from the Hamiltonian, H, and overlap, S, matrices of the extended molecule for each applied bias voltage, V, as (for clarity we have removed the V dependence in all equations)

$$G_M(E) = [ES_{MM} - H_{MM} - \Sigma_L(E) - \Sigma_R(E)]^{-1}, \quad (1)$$

$$\Sigma_X(E) = (ES_{MX} - H_{MX})g_X(ES_{XM} - H_{XM}), \quad X = L,R, \quad (2)$$

where subscripts X and Y in H_{XY} and S_{XY} (submatrices of H and S, respectively) refer to the molecule (M), left contact (L), and right contact (R). The self-energy function Σ_X accounts for the coupling between contact X and the standalone molecule; it contributes to the shifting and broadening of the molecular levels and depends on the Green's function of the contact, g_X, which is given by

$$g_X(E) = \pi i \begin{bmatrix} g_{X1} & \cdots & 0 \\ \vdots & \ddots & \vdots \\ 0 & \cdots & g_{XN_X} \end{bmatrix}, \quad (3)$$

$$g_{XK}(E) = \begin{bmatrix} (Ds)_{XK}(E) & 0 & 0 & 0 \\ 0 & (Dp)_{XK}(E) & 0 & 0 \\ 0 & 0 & (Dd_{t_{2g}})_{XK}(E) & 0 \\ 0 & 0 & 0 & (Dd_{e_g})_{XK}(E) \end{bmatrix}. \quad (4)$$

The diagonal entries of $g_{XK}(E)$, from top to bottom, give the $s, p, d_{t_{2g}}, d_{e_g}$ contributions to the DOS of contact-atom K. The number of contact-atoms is such that the size of $g_X(E)$ equals the number of columns (rows) of the coupling matrix H_{MK} (H_{KM}).

The transmission function (T) and the DOS (D) are obtained from the relations

$$T(E) = \mathrm{Tr}(\Gamma_L(E)G_M(E)\Gamma_R(E)G_M^+(E)) \quad (5)$$

$$D(E) = \mathrm{Tr}(i[G_M(E) - G_M^+(E)]S), \quad (6)$$

where $\Gamma_X(E) = i(\Sigma_X(E) - \Sigma_X^+(E))$. $T(E)$ is the sum of the transmission probabilities from each of the channels available at energy E. In consequence, the current $I(V)$ at a bias voltage V is obtained from

$$I(V) = \frac{2e}{h}\int_{-\infty}^{\infty} dET(E)(f_L(E - eV/2) - f_R(E + eV/2)) \quad (7)$$

with f_X denoting the Fermi-Dirac function at contact X.

III. RESULTS AND DISCUSSIONS

For the sake of practical solvability, the molecular junctions are initially approximated by the extended molecules **3**, **4**, and **5**, in which the electrodes are included as small clusters of sizes of up to three Pd or Au atoms. This is a reasonable approximation since the characteristics of a molecular junction converge well when very few metallic ending atoms are used in the calculations [5,37–39]. The extended molecules are then linked at their ends with semi-infinite metallic leads of similar atoms as those at their endings. For these final configurations we obtain the I-V characteristics which together with all the information gathered in the previous steps allow us to give a complete account of the events leading to the observed bistability phenomenon in the oligoaniline molecular junction.

A. Molecular structures

Three distinctive types of conformational isomers, designated α, β, and γ, are found for the oligoaniline **1**. Each type has many different isomers, two of which are depicted in Fig. 4, namely, α: **6** and **6′**, β: **8** and **8′**, and γ: **7** and **7′**. For example, **6′** is obtained from **6** by rotating the latter left α-phenyl-N-methyl substructure an angle of $\sim 90°$ around the N7-C1 bond (notation is as in **1**, Fig. 1). An oligoaniline

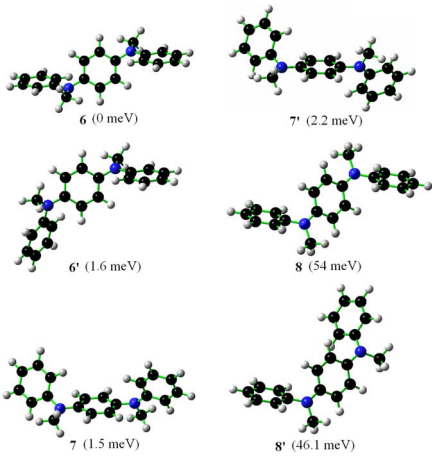

FIG. 4. (Color online) Stable conformations of the oligoaniline **1**: **6** and **6′** are isomers in α conformation; **7** and **7′** are isomers in γ conformation; and **8** and **8′** are isomers in β conformation. The isomers' energies shown in parentheses are with respect to the α conformation **6**. Each primed configuration is obtained from the unprimed one by a rotation of one of the exterior-phenyl-N-methyl substructures around the adjacent N-C bond joining the substructure N atom to the central phenyl.

TABLE I. Bond lengths (Å), bond angles (degrees), and dihedral angles (degrees) of a selected set of optimized oligoaniline conformational isomers

Parameter	α (**6**)	β (**8**)	γ (**7**)	α (**6′**)
H14-H6	2.824	2.818	2.765	2.782
H5-H22	2.823	2.818	2.873	2.781
C9-N7	1.399	1.416	1.418	1.398
C1-N7	1.419	1.405	1.398	1.418
C8-N7	1.452	1.452	1.452	1.452
C12-C20	12.431	12.430	11.645	11.370
C9-N7-C8	118.9	117.4	117.5	118.9
C1-N7-C8	117.2	118.3	118.7	117.3
C9-N7-C1	121.0	120.7	121.3	121.2
C4-N15-C16	117.2	118.3	116.9	117.3
C17-N15-C16	118.9	117.4	119.2	118.9
C4-N15-C17	121.0	120.7	121.0	121.2
C10-C9-N7-C8	−8.8	58.2	−58.9	−8.7
C14-C9-N7-C8	168.3	−120.8	119.7	168.3
C2-C1-N7-C8	−61.7	12.9	−10.2	−61.0
C6-C1-N7-C8	116.6	−163.9	166.7	117.2
C3-C4-N15-C16	−116.6	164.0	110.6	−60.9
C5-C4-N15-C16	61.7	−12.9	−67.3	117.3
C18-C17-N15-C16	8.8	−58.2	−5.3	−8.7
C22-C17-N15-C16	−168.3	120.8	172.2	168.4

structural isomer will be called α conformation, if both of its methyl groups are (almost) coplanar with the (exterior) α-phenyls; β conformation, if the methyl groups are in (almost) coplanar conformation with the (central) β-phenyl; and γ conformation, if one of the methyl group is (almost) coplanar with an α-phenyl and the other is so with the β-phenyl. Typical geometrical parameters for conformers of the three types are listed in Table I.

Our calculations show that the α conformer **6** has the lowest conformational energy (0 meV—our reference energy) and the β conformer **8** the highest (54 meV). The energies of the γ and α conformations are spread over a range of only a few meV from the reference energy: **6**, 0.0 meV; **6′**, 1.6 meV; **7**, 1.5 meV; and **7′**, 2.2 meV. This shows that the potential energy landscape of the standalone oligoaniline is rather flat around our zero energy. By contrast, the energies of the β conformers are above 46 meV and well separated from each other: **8**, 46.1 meV; **8′**, 54 meV. It can be estimated that there are about 48%, 7%, and 45% of the molecules in the α, β, and γ conformations, respectively, when equilibrium is reached at room temperature (25 °C).

Conformations differences have a large effect on the electron transport properties of molecular junctions, and conformational changes have been used to explain molecular diode behavior [4,40] and the bistability (or switching) observed in some molecular junctions [3,6,7,10,34,41]. Since, as discussed above, the conformational energies of many of the oligoaniline isomers are only a few meV, an external electric field induced by the bias voltage applied to the junction can easily cause conformational changes on the oligoaniline (see Sec. III F), affecting in this way its conformational distribution. As a result, switch between different conductivities is expected in an oligoaniline molecular junction.

B. Electronic structure of oligoaniline

The molecular orbitals shapes and energies for the three types of conformational isomers of oligoaniline **1** are shown in Fig. 5. Although the total energies of these isomers may be very similar, the energies of their orbitals may be quite different, especially those of the HOMO (highest occupied molecular orbital) and LUMO (lowest unoccupied molecular orbital). A methyl coplanarity with an α-phenyl (methyl in α-conformation) tends to decrease the HOMO and LUMO energies; whereas its coplanarity with a β-phenyl (methyl in β conformation) has the opposite effect. Since an α isomer has two methyl groups in α conformation, then it has the lowest HOMO and LUMO energies. The β isomer, on the other hand, having two methyl groups in β conformation, has the highest HOMO and LUMO energies. The γ isomer HOMO and LUMO energies lie somewhere between those of the α and β isomers. These changes in HOMO and LUMO energies caused by conformational isomerization will greatly affect their relative conductivities, and are one of the major mechanisms which may cause bistable states on the oligoaniline molecular junction as observed in experiments [7].

In all the isomers, the HOMO is more delocalized than the LUMO as well as well delocalized through the entire molecule. A fully delocalized orbital is usually considered a good conduction channel [42–45]; therefore, it is reasonable to expect that the oligoaniline molecular junction has a hole-conduction mechanism, in which, the conduction is induced by the positively charged holes injected from a metal electrode into the HOMO of the molecule. In a more realistic picture, each molecular orbital, occupied and unoccupied, contributes to the electron transport according to their separation from the Fermi level and to their spatial shapes [32,46]. To analyze this point further, we next consider the molecular energy levels of an extended oligoaniline molecule.

C. Electronic structure of the extended oligoaniline molecule

Figure 6 shows the energy level diagrams of the conformations of the extended molecule Au_2-**5**-Pd_2. Unlike the molecular orbital diagrams of **1**, Fig. 5, the Fermi levels of the extended molecule conformations are rather similar, with the existence of much more allowable state energies close to the Fermi levels of bulk Au and Pd due to the addition of the contact atoms. This addition also shifts downwards the Fermi level of **1**, assumed to be located at the center of its HOMO-LUMO gap, towards the Fermi levels of bulk gold and palladium. In particular, the α conformers have the HOMOs with the lowest energies, **6′** (−4.92 eV) and **6** (−4.94 eV), and γ, **7**, has the smallest HOMO-LUMO gap, 0.64 eV, with α, **6′**, having the largest, 0.91 eV. Such as for the standalone oligoaniline, our calculations (not shown) indicates that the HOMO of the extended molecule is more delocalized than the LUMO, which is localized at the Au-S interface, and has better coupling in the S-Pd interface than in the S-Au. That

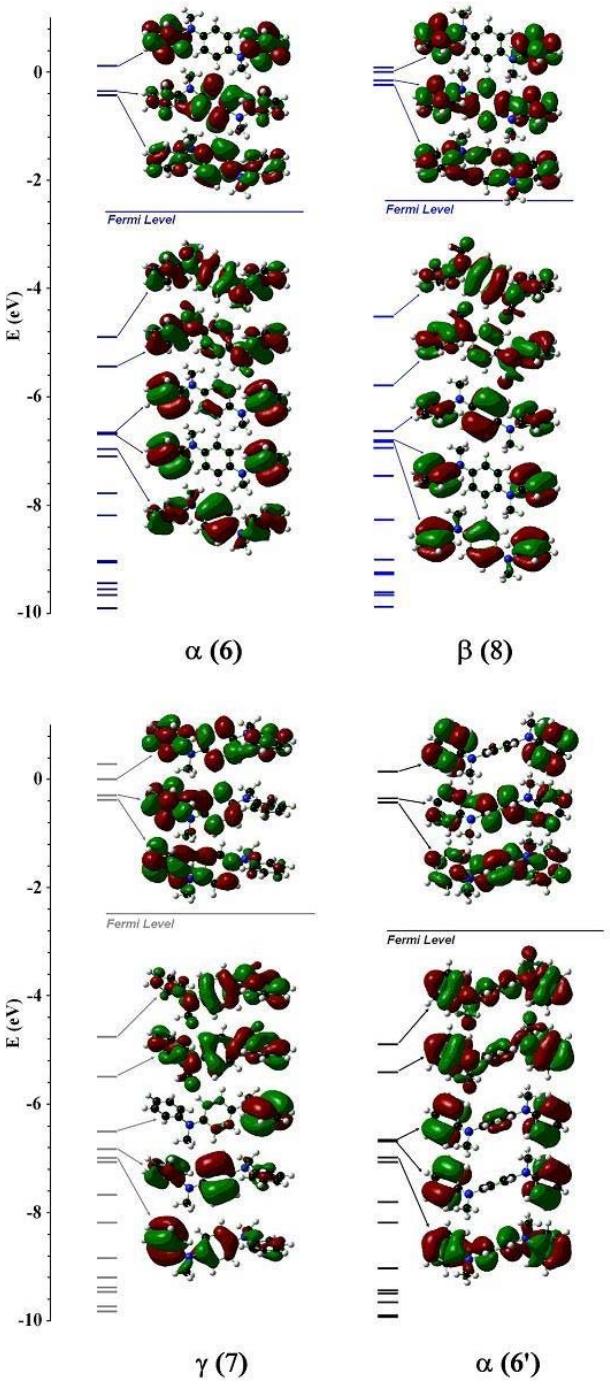

FIG. 5. (Color online) Zero-field molecular orbital energies and orbitals for the α (**6** and **6′**), β (**8**), and γ (**7**) conformers of the oligoaniline **1**. The Fermi energies are calculated as the center of the HOMO-LUMO gap.

S-Pd is a better interface than S-Au for charge transport was theoretically suggested [33] and experimentally corroborated [47]. Therefore, the HOMO is a better conduction channel than the LUMO, suggesting that charge transport in the oligoaniline junction $Au_{bulk}Au_2$-**5**-Pd_2Pd_{bulk}, as well as in Au_{bulk}-**5**-Pd_{bulk} and $Pd_{bulk.}$-**3**-Pd_{bulk}, occurs mainly via hole injection from the Pd lead to the HOMO level of the molecule.

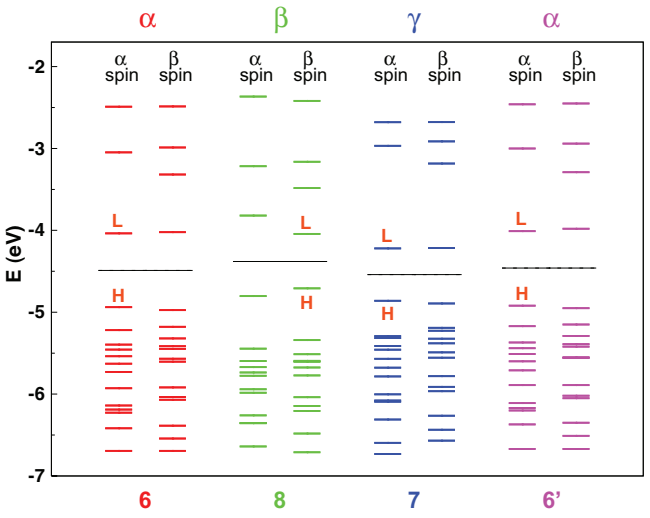

FIG. 6. (Color online) Allowable energy levels for α(**6** and **6′**), β (**8**), and γ (**7**) configurations of the Au_2-**5**-Pd_2. The long horizontal black bars indicate the Fermi level of the molecules.

D. DOS and TF of fixed oligoaniline molecular junctions

In our calculations we have considered both a symmetric junction with Pd electrodes as well as an asymmetric one with Au and Pd electrodes. In the former, the standalone oligoaniline has been extended with one electrode atom at each end, whereas in the latter it has been extended with either one or three such atoms; in all cases sulfur atoms have been used as clippers. These extensions should help obtain an adequate qualitative picture of the *I-V* characteristics of the junctions. Indeed, some calculations have found that the on-top contact structure is stable for both regular and irregular electrode surfaces [48] with modifications in the atomic contact geometry leading to a slight shift of the conductance peaks; although chemical intuition and our calculations suggest that regular surfaces would be unstable. Other analysis of the on-top contact structure with different topological neighborhoods yielded that the single gold atom interacting directly with the molecule played the most important role in the *I-V* characteristics of the junction [5,49].

When an isolated oligoaniline molecule is connected to the contacts via the S clippers, its discrete states are broadened and shifted, as illustrated in Fig. 7 for the α spin of an α conformer of the oligoaniline, **6′**, in the asymmetric junction, $Au_{bulk}Au_2$-**5**-Pd_2Pd_{bulk}. The broadening of the density of states (DOS) depends on the strength of the coupling to the contacts and on the wave function of the considered state [32]. As seen in Fig. 7 (top panel), the peak of the HOMO is broader than that of the LUMO, indicating a greater coupling strength of the former. This can be explained by looking at the frontier molecular orbitals of the extended molecule Au_2-**5**-Pd_2 of **6′** (not shown), which reveals that the HOMO is delocalized throughout **6′** and the metal contact interfaces whereas the LUMO is localized around the gold contact interface and neighboring ring. The energy states of the bare **6′** and its extended molecule Au_2-**5**-Pd_2 are depicted in the bottom and middle panels, respectively, of Fig. 7; in either case the HOMO is indicated by H and the LUMO by L. The

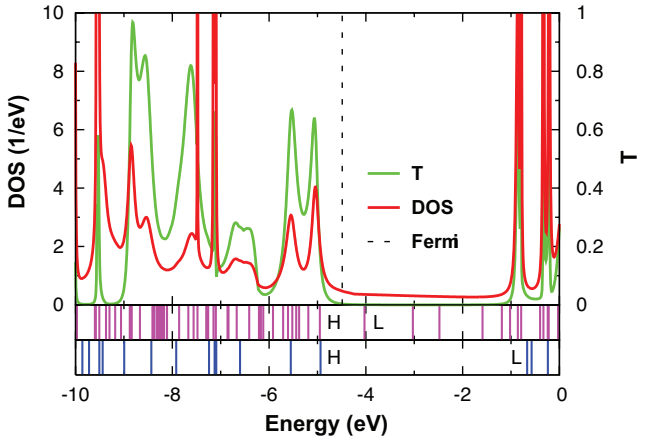

FIG. 7. (Color online) Zero-bias transmission function and DOS for the alpha spin of molecule **6′** in an Au_2-**5**-Pd_2Pd_{bulk} junction (top panel). Also shown are the discrete energy levels of **6′** when isolated (bottom panel) and when extended as Au_2-**5**-Pd_2 (middle panel), indicating in either case the HOMO and LUMO energies. The Fermi line in the top panel corresponds to the average of the HOMO and LUMO energies of the extended **6′**. All calculations are done at the B3PW91/LANL2DZ level of theory.

molecular orbitals of Au_2-**5**-Pd_2 are linear combinations of orbitals of Au, Pd, S (the clipper) and **6′**. As listed in Table II, its HOMO sits at −4.94 eV, nearby the HOMO of **6′**, located at −4.92 eV; whereas its LUMO sits at −4.01 eV, far apart from the LUMO of **6′**, located at −0.67 eV. Indeed, an analysis of the contributions of the molecular orbitals of the extended molecule component atoms to the HOMO and LUMO [50] yields, S: 0.14, Au: 0.06, Pd: 0.14, and **6′**: 0.66, for the HOMO, and S: 0.08, Au: 0.87, Pd: 0.00, and **6′**: 0.05, for the LUMO. In consequence, the HOMO is mainly a **6′** molecular orbital, it is in fact the **6′** HOMO shifted by 0.2 eV, and that the LUMO is, to all purposes, an Au molecular orbital. As a matter of fact, the first **6′** molecular orbital to the right of the HOMO lies at about −0.83 eV, with a population composition of S: 0.01, Au: 0.01, Pd: 0.02, and **6′**: 0.96. This is the **6′** LUMO which has been shifted by ∼−0.16 eV. In this case, both the total density of states (DOS) and transmission functions (top panel) peak around the states of the isolated molecule (bottom panel).

Figure 8 shows the zero-bias DOS, panels (a-c), and transmission function, panel (d), for three conformations of molecule **3** in the symmetric junction, Pd_{bulk}-**3**-Pd_{bulk}. The Fermi line in a panel refers to the average of the HOMO and LUMO of a conformation of **3**. In the calculations, the 6-31G basis set was used for all atoms except S and Pd, for which the LANL2DZ basis set and effective core potential were used. Panels (a-c) reveal strong hybridization between the molecular orbitals and the extended states of bulk Pd due to the covalent bond between Pd and S. For each conformation there is a gaplike structure for the transmission, and DOS at about −2.8 eV. In addition, the shape of the total transmission resembles closely that of the DOS and both of them peak around the energy levels of the isolated molecule shown in the bottom panels in (a-c).

TABLE II. The total energy and the HOMO and LUMO energies of the isolated oligoaniline in conformation α (**6′**) and its extended molecules: with single-particle clusters of Au and Pd, **5**, and with trimer clusters of the same metals, Au_2-**5**-Pd_2. Also listed is the HOMO-LUMO gap for each of the molecules. The column "cluster size" lists the size of the extending clusters.

Molecule	Cluster size	Energy (Ha)	HOMO (eV)	LUMO (eV)	Gap (eV)
6′	0	−883.19712	−4.94	−0.67	4.27
5	1	−1164.54463	−5.15	−3.47	1.68
Au_2-**5**-Pd_2	3	−1689.24547	−4.92	−4.01	0.91

E. Current-voltage characteristics at fixed geometries

Current-voltage calculations for the junction Pd_{bulk}-**3**-Pd_{bulk} have been carried out with molecule **3** fixed at its energy optimized geometries α (**6**), β (**8**), and γ (**7**); the results are displayed in Fig. 9. The energies of these conformers of **3** relative to that of its most stable conformer, α (**6**), are: α (**6**), 0 meV; β (**8**), 34 meV, and γ (**7**), 18 meV. It is then reasonable to expect that when equilibrium is reached at room temperature, α has the highest probability to be found in the junction and β has the lowest. In spite of this latter characteristic of β and of its high instability under the action of an applied external voltage (when molecular structural changes are taken into account, see Sec. III F), we show, nevertheless, its *I-V* curve in Fig. 9 to compare it with those of the other conformers. It follows that overall β carries the highest current over the voltage range $|V|<5.0$ V. Moreover, for voltages $|V|<\sim 2.3$ V, α and γ carry very similar currents; outside of this range, γ carries the higher current, until ±4.5 V, after which points α becomes the higher current carrier. Given that α has a much higher probability than γ to be found in the junction at room temperature, the above evidence suggests a possible scenario for understanding the experimentally observed current switching between low and high current states in a Pd_{bulk}-**3**-Pd_{bulk} junction [7], and also in the other oligoaniline junctions [7], at room temperature, namely, conformational switching between α and γ, under the action of an applied bias potential with α carrying the low current and γ the high. Although the conformational switching scenario was already suggested [7], here we name the conformations involved in the switching, and in the next section will give, through a simple model calculation, concrete evidence supporting the role of these conformations in the hysteretic behavior of the oligoaniline junction. In this preliminary assessment we have neither consider structural changes in the sandwiched molecule, nor general charging effects, nor molecular screening for that matter.

F. Conformational changes under applied electric fields

We have performed geometry optimizations of the conformations of a neutral molecule **5** in the presence of an electric field to test their stability under the action of an applied external field. All optimizations have been done at the B3PW91/LANL2DZ level of theory, with fields directed along the z-axis as indicated in Fig. 10.

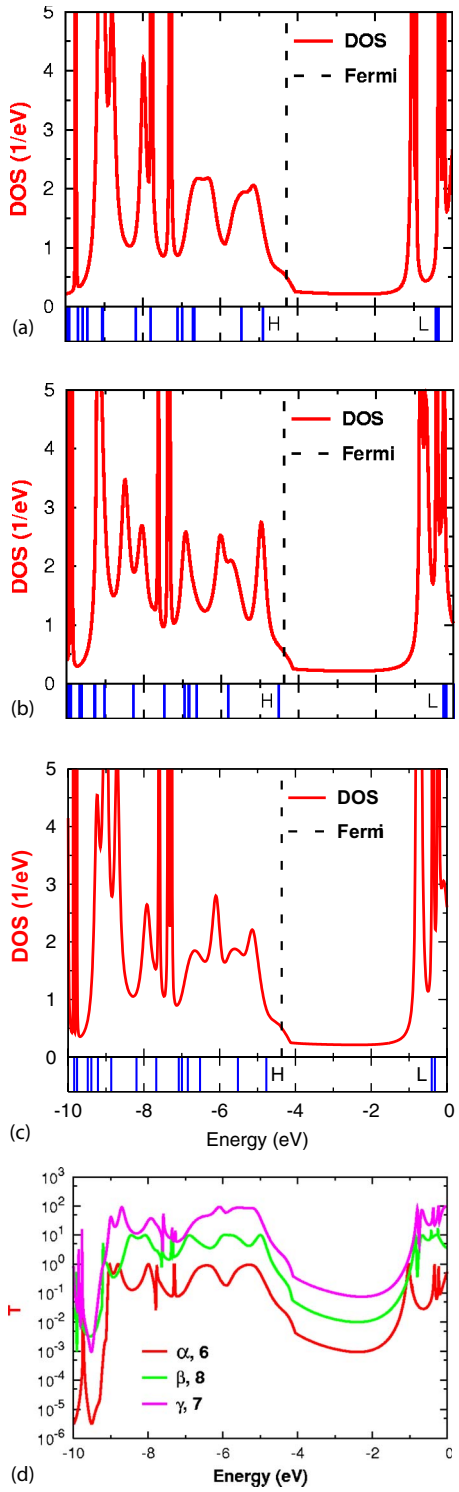

FIG. 8. (Color online) (a–c) Top panels: DOS for the (a) α (**6**), (b) β (**8**), and (c) γ (**7**) conformations of oligoaniline **1** in the Pd_{bulk}-**3**-Pd_{bulk} junction. The Fermi lines denote the Fermi levels of the corresponding conformers of **3**. Bottom panels: discrete energy levels of the (a) α (**6**), (b) β (**8**) and (c) γ (**7**) conformers of **1** indicating in each case the HOMO (H) and LUMO (L) energies. The transmission functions of the conformers of **1** in the junction are shown in logarithmic scale in panel (d). For better visualization the curves have been shifted upward by consecutive powers of ten. Top (purple) curve corresponds to γ (**7**), middle (green) curve to β (**8**), and lower (red) curve to α (**6**).

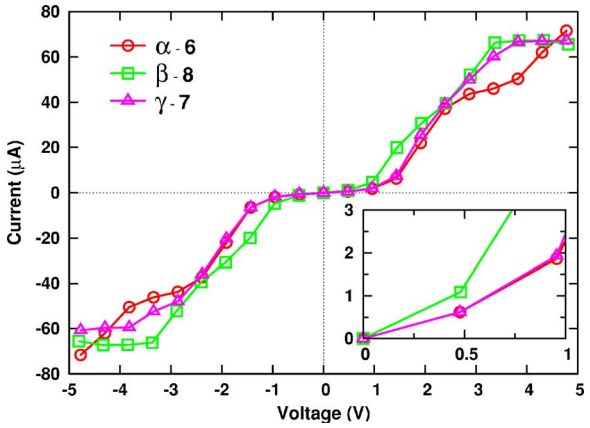

FIG. 9. (Color online) *I-V* characteristics of the α, β, and γ conformations of oligoaniline **1** molecular junction Pd_{bulk}-**3**-Pd_{bulk}. The inset highlights the currents for small positive bias voltages.

For comparison, in Table III we show the energies of the zero-field optimized conformers α (**6**), β (**8**), γ (**7**), and α (**6′**) for the standalone, **5** and Au_2-**5**-Pd_2 molecules. For each molecule, the energies are given relative to the energy of α (**6**), the most stable conformer. As can be seen from the table, the relative energy of α (**6′**) is of just a few meV and fairly stable upon addition of a few extending atoms. In contrast, the relative energies of β (**8**) and γ(**7**) are at least an order of magnitude larger than those of the α in spite of their large fluctuations. Although the data set is small to establish a definite pattern for the stabilization of the energy as a function of the number of the extending atoms, nevertheless it suggests relative energies for β and γ that are many times over those of the α, with β energy being the largest. It then follows that to a first approximation (i.e., considering few extending atoms), when equilibrium is reached, the α conformation has the highest probability to exist at room temperature, β has the lowest. In fact, we shall see later on that for molecule **5**, β is also unstable under the action of an external applied field. Table III also suggests that by considering the extended molecule **5** in our optimization calculations, we are most likely using upper bound relative energies for the extended molecules.

Now, the optimization runs are done for positive and negative fields, starting in either case at zero-field and incrementing the field strength in steps of 0.0005 a.u. until 0.0035 a.u.. The molecule optimized geometry as well as its wave function is used as input for the optimization at the next higher positive (lower negative) field. For example, the zero-field optimized α conformer is used as input for the optimization at 0.0005 a.u.. This procedure is repeated until the end of the run, in the positive direction in this example. Since the field strength is given by $F=V/L$, where L is the length of the (extended) molecule, then it may yield different bias voltages depending on the length of the molecule considered. Moreover, as our sampling of field strengths is rather coarse, it is not possible to tell exactly at which field strength a conformational change actually takes place. We have thus assigned the switching point to the first point in our grid where this occurs, the actual switching point possibly being at a smaller strength. For the range of bias applied fields

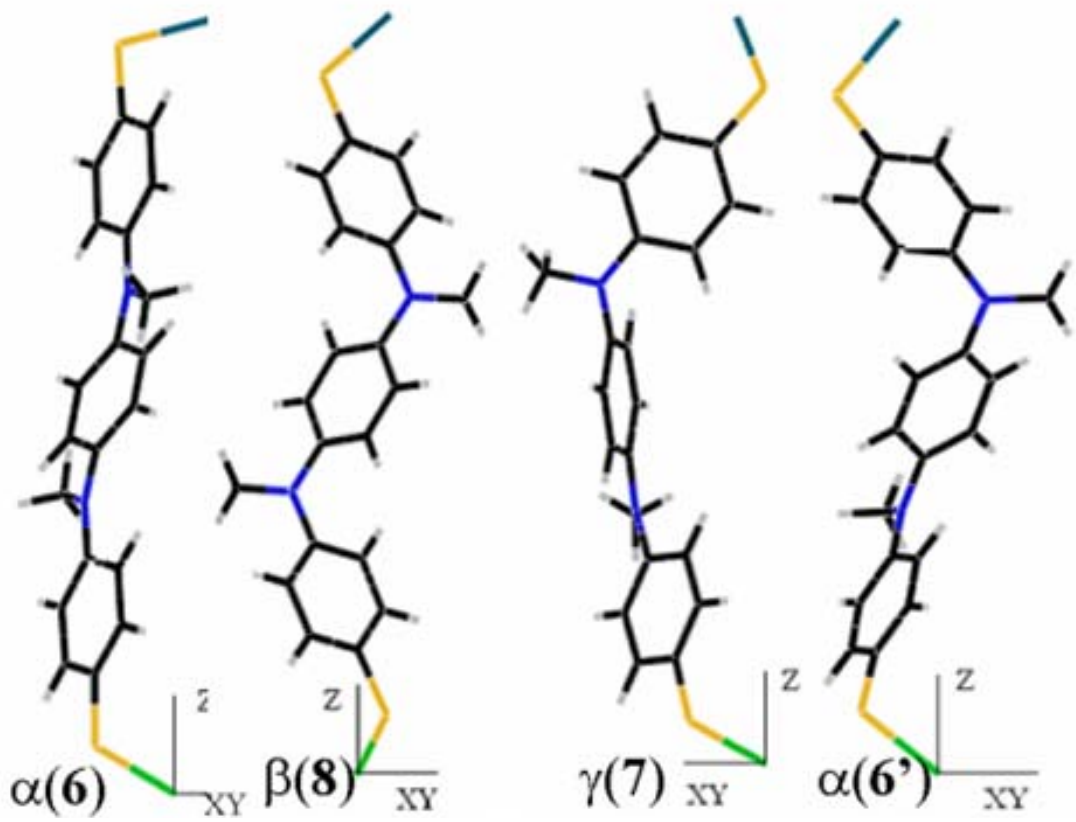

FIG. 10. (Color online) Zero-field stable conformations of the extended molecule, **5**, of the oligoaniline: α (**6**), β (**8**), γ (**7**), and α (**6′**). Field optimizations of these conformers are carried out with the field applied along the z axis. In all cases the xy plane is orthogonal to the plane of the figure.

spanning from −0.0035 to 0.0035 a.u., we find that α and γ are the most likely conformations to be found in a given sample, see Fig. 11. By this we mean that the geometry of a conformation satisfy the overall geometrical characteristic of the α or γ configuration as defined in Sec. III A, e.g., the methyl groups are (almost) coplanar with the α-phenyls in an α configuration; but undoubtedly some of the molecules' dihedral angles as well as spatial dimensions will change with the applied field. At low fields, $|F|<0.001$ a.u., say, most of the visible changes will take place at the S-Au and S-Pd interfaces, though drastic changes in the molecule geometry may occur, as is the case for the β conformation, Fig. 11. Increasing the magnitude of the applied field, however, will make apparent the changes taking place in the internal dimensions of the molecule. Although our *ab initio* calculations for the conformational changes of the extended oligoaniline under field take into account all these considerations, for a practical description of conformational changes, we

TABLE III. Zero-field energies of the optimized conformers α (**6**), β (**8**), γ (**7**), and α (**6′**) of the standalone, **5** and Au_2-**5**-Pd_5 molecules. All energies are given relative to the energy of the most stable conformer, α (**6**). The column "extending cluster size" lists the size of the extending metallic clusters at each end..

Molecule	Extending cluster size	Energy α (**6**) (meV)	Energy β (**8**) (meV)	Energy γ (**7**) (meV)	Energy α (**6′**) (meV)
Standalone	0	0	61	3	1
5	1	0	89	34	1
Au_2-**5**-Pd_2	3	0	56	17	4

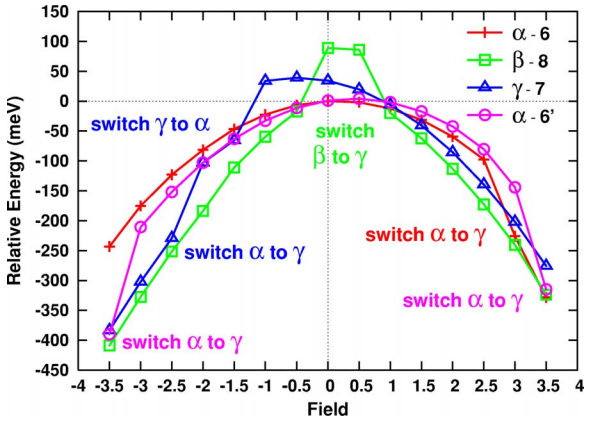

FIG. 11. (Color online) Electric field effects on the energies of the conformations of molecule **5**. All energies are relative to that of the most stable conformation at no field, namely α (**6**). Field sweeps are done for positive and negative fields, starting in either case at zero field. Plus signs, open circles, open triangles and open squares refer to data for the α (**6**), α (**6′**), γ (**7**), and β (**8**) conformations, respectively. The switching points of the conformers (see text) are indicated by a text "switch x to y" alongside the points. Electric field is in 10^{-3} a.u. (1 a.u.=51.423 V/Å).

have chosen to emphasize the role of the relative positions of the methyl groups with respect to the α- and β-phenyl groups in the molecule, that is, the role of changes in the dihedral angles of the molecule.

As we pointed out in Sec. III A, at zero-field many conformers are available for each conformation type. They essentially differ by the dihedral angles each of their methyl groups makes with its neighboring α- and β-phenyl rings; which in turn implies they have different lengths. We can use, for instance, the set of dihedral angles C6-C1-N7-C8, C10-C9-N7-C8, C5-C4-N15-C16 and C18-C17-N15-C16 (notation is as in Fig. 1) to specify the conformers. For example, the optimized α conformer **6** of **5** would be specified by the angles 121.5°, −10.4°, 53.6°, and 11.0°, whereas the optimized **6′** would be so by 120.7°, −9.3°, 122.9°, and −10.8°. Although this scheme yields a systematic procedure to label the conformers, its use to follow the evolution of a conformer geometry under the action of a field would be tedious as in this case the dihedral angles will regularly change. Instead, we choose to label a conformer by its type, indicating, whenever possible, the molecule in Fig. 4 that best resembles it; especially in regards of the above set of dihedral angles. Thus, we write, for example, "∼**6**" to denote a conformer whose geometry is close to that of **6**. This scheme is both simple and sufficient for our goal of describing the conformational changes of the extended oligoaniline.

Figure 11 summarizes our results for the energy changes under field of the conformations of molecule **5**. The quoted energies are relative to the energy of the most stable conformer, α (**6**), at zero-field [10]. We see that for negative fields, the energy of the α conformers decreases smoothly as the field strength increases, with **6′** having slightly lower energy than **6**. At a field of −0.003 a.u., however, the energy of **6′** falls sharply signaling a change of conformation to γ at −0.0035 a.u.; in contrast, **6** does not flip within the range of negative fields studied. The energy of the β conformer, on the other hand, drops sharply on going from zero field to −0.0005 a.u., whereupon β switches to a γ conformation (∼**7′**), whose energy steadily decreases as the strength of the negative field increases, remaining at a lower energy than those of the other conformers. The energy of the γ conformer, **7**, increases slightly at first reaching its maximum at −0.0005 a.u., it then decreases slowly until abruptly diving at −0.001 a.u. signaling the flipping of γ to α (∼**6′**) at −0.0015 a.u.. Further increase of the field strength brings about a second steep decrease in energy at −0.002 a.u. leading to α switching conformation back to a γ' (∼**7′**) at −0.0025 a.u.. For positive fields, the α conformer, **6**, has a slightly higher energy than **6′**, with both conformers flipping to a γ conformation (∼**7′**), the former at 0.003 a.u. and the latter at 0.0035 a.u.. These flips are signaled by sharp energy drops, at 0.0025 a.u. for **6**, and at 0.003 a.u. for **6′**. The energy of the β conformer, on the other hand, decreases slowly at first before taking a steep dive at 0.0005 a.u., leading to β flipping to a γ conformation at 0.001 a.u. The energy of this latter conformation decreases smoothly for increasing field strength, remaining the lowest of all conformers' energies. Finally, the energy of the γ conformer, **7**, follows a smooth and monotonically decreasing curve for increasing field strengths.

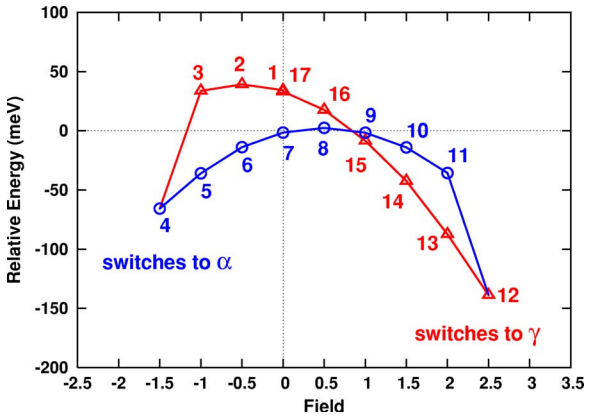

FIG. 12. (Color online) Effect of the bias electric field on the energy of a γ conformer of **5**. The sweep starts at zero field, point 1, with a γ conformation, and heads in the direction indicated by the sequence of numbers. At point 4 the molecule changes conformation from γ to α, switching back to a γ conformation at point 12. The molecule is in γ conformation at the open triangle points and in α conformation at the open circle points. All the energies are relative to the energy of the α (**6**) conformer at zero field. Electric field is in 10^{-3} a.u. (1 a.u.=51.423 V/Å).

In summary, in the negative field regime there are only two conformations of the oligoaniline present, α and γ and this is also the case in the positive field regime, save for fields below about 0.0005 a.u. where the β conformer is also present. Moreover, a closer look in Fig. 11 at the energy changes and switching points of the α and γ conformations reveals some hints of hysteretic phenomenon in the energy of **5**. Indeed, for moderate positive fields both α conformers switch to a γ conformation, whereas for low negative fields the γ conformer switches to an α conformation. These changes are further explored in Fig. 12.

To investigate the hysteretic behavior of the energy of **5**, we carry out on **5** a full round of geometry optimizations under field (Fig. 12), starting and ending at zero-field (points 1 and 17, respectively, in Fig. 12). We start with **5** in γ conformation (**7**), and as before, the optimized geometry and wave functions obtained at one point in the circuit are used as input in the optimization run at the next point. When the field is swept from 0 to −0.0015 a.u, the energy of **5** follows a smooth arc until taking an sharp dive at −0.001 a.u. (point 3) leading to a switch of conformations, from γ to α, at a negative threshold field (F_T^-) of −0.0015 a.u. (point 4). **5** remains in this α conformation state on sweeping the field upward from −0.0015 a.u., through zero field (point 7), until 0.002 a.u. (point 11), at which point its energy once again suddenly jumps down, leading to **5** switching back to a γ conformation at a positive threshold field (F_T^+) of 0.0025 a.u. (point 12). Likewise, once **5** is in the γ conformation state, it will remain in this state until sweeping the bias field down to the negative field threshold (points 12-17; the remaining two points are not shown). Furthermore, once **5** is brought to a threshold field, lowering the field to −0.002 a.u. from the negative threshold, or increasing the field to 0.0035 a.u. from the positive threshold, will keep its state unchanged, as can be deduced from the α- and γ-curves in Fig. 11. As can be seen in Fig. 12, the path described by the relative energies is

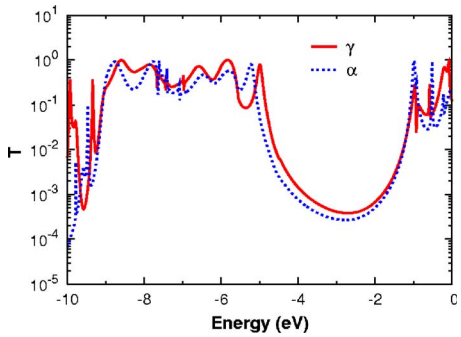

FIG. 13. (Color online) Transmission functions for the α spin of the γ, solid (red) curve, and α, dotted (blue) line, conformers of **5** at points 3 and 5, respectively, of Fig. 12 (see also Fig. 14).

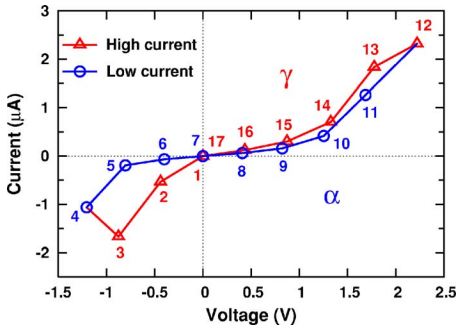

FIG. 14. (Color online) Hysteretic behavior of the current in an oligoaniline junction Au_{bulk}-**5**-Pd_{bulk} under the action of a bias potential. Open triangles refer to high-current data, open circles to low-current data. The junction is in a high-current state when the oligoaniline is in γ conformation and in a low-current state when the oligoaniline is in α conformation. The sequence of points indicates the direction of the voltage sweep and is the same as that of Fig. 12. The solid lines are guides to the eye.

almost closed; the energy at the ending point 17 is lower than that at the starting point 1 by just 1.09 meV, an about 3% relative energy decrease. This path describes a typical hysteretic curve for the extended molecule **5**.

An immediate question then arises as to what happens to the current through the junction as the molecule follows its hysteretic path. To answer this question, we have used Eq. (7) of Sec. II C to compute the current through the junction at each point of the hysteretic curve depicted in Fig. 12. Our results for the *I-V* characteristics of the junction, displayed in Fig. 14, show that the oligoaniline junction Au_{bulk}-**5**-Pd_{bulk} exhibits a hysteretic switching behavior as found experimentally in [7]. Indeed, the junction is in its high current state (red curve) when the oligoaniline is in γ conformation, and is in its low current state (blue curve) when the oligoaniline is in α conformation. Furthermore, the positive voltage threshold (V_{T+}) for switching from low to high current is ~ 2.2 V, and the negative voltage threshold (V_{T-}) for the reverse switching is ~ -1.2 V; these voltage thresholds correspond to the positive, F_T^+, and negative, F_T^-, field thresholds, respectively, introduced earlier. Although the hysteretic strength shows weakly for positive voltages, it does show quite strongly for negative voltages. In particular, for instance, Fig. 13 shows that for the hysteretic curve in Fig. 14, the γ conformer at point 3 has an overall higher transmission function, with a narrower gap, than that of the α conformer at point 5. These transmission functions are obtained at an applied field of 0.001 a.u. before and after the switching from γ to α. The above characteristics are consistent with the finding in Fig. 14 that the current at point 3 is higher than the current at point 5.

Our aim throughout this section has been to explore the qualitative aspects of the experimental results in [7], still we feel it is a good idea to compare some of the quantities that can be extracted from our calculations with those measured in Ref. [7] more than anything else, as an attempt to come to grips with the limitations of such comparisons. First, our calculated currents span a range of values twice as large as that of the experimentally measured values: from ~ -2 to ~ 2.5 μA, for the former, and from -0.6 to 1 μA, for the latter. Still, they are of the same order of magnitude as the measured ones, and the discrepancies are hardly surprising in view that the measured current corresponds to that of an Au-SAM(oligoaniline)-Pd junction whereas the computed current correspond to that of a single molecule oligoaniline junction. Notice that, at this point, there is no way to experimentally find out how many molecules were conducting. Moreover, the measured threshold voltages for current switching were, $V_{T-} = \sim -1.5$ V and $V_{T+} = \sim 1.5$ V, whereas the computed values were, $V_{T-} = -1.2 \pm 0.4$ V and $V_{T+} = 2.2 \pm 0.5$ V, where in the latter account has been taken of the size of the field mesh used. Again, the agreement seems remarkable, especially when considering the abundant randomness in the experimental settings.

In summary, we have argued and shown that the conformational switching scenario could very well explain the experimentally observed bistable switching in nanoscale thiol-substituted oligoaniline molecular junctions [7].

Finally, a possible point of concern is that the contacts constrain considerably the movements of the molecules, as well as the SAM environment used in the experiments; thus suggesting that at least the metal atoms should be constrained during optimizations with the applied electric field. Although, this seems very logical, it has been proved, at least for gold theoretically [51] and experimentally [52] that atoms on the gold surface are not better attached than atoms in an organic molecule. Gold atoms may be attached to the surface through one gold atom with energies of ~ 40 kcal/mol as opposed to the bonds on the molecule whose energies are of ~ 80 kcal/mol. Macroscopically we might think of a hard tip attached to a floppy molecule, atomistically we have a strong molecule attached to flexible gold atoms. An analysis of the atomic lengths from the molecule to the metal atoms yield root-mean-square displacements with respect to their neighbor atoms in the molecule of ~ 0.1 and 0.3 bohr for Au and Pd, respectively, per (10^{-3} hartree e^{-1} bohr^{-1}) of applied electric field.

IV. CONCLUSIONS

We have presented a theoretical study of the structural and electronic properties of the oligoaniline molecule. We found three types of nonplanar conformations, α, β, and γ, for the

neutral isolated and extended oligoaniline. α and γ types have nearly equal energies and are more stable than the β type. Each conformation type presents several conformers whose energies have about the same value. On an extended oligoaniline, switching between conformations α and γ can be obtained by applying an external voltage to the molecule. These switching takes place producing a hysteretic phenomenon in the relative energies for these two conformers.

Charge transport in the oligoaniline junction occurs via hole conduction due to the metal electrodes coupling to the molecule HOMO level which is delocalized throughout the molecule. This makes the HOMO a better conduction channel than the LUMO, which is localized around the Au-S interface.

Although we feel this preliminary study gives a reasonable theoretical picture of the oligoaniline molecular junction, there are still several issues to resolve to completely understand and use these junctions in a molecular electronics scenario determining whether the hysteretic phenomenon can still be clearly observed when the oligoaniline molecule is arranged in a molecular circuit. This certainly requires of concerted theoretical and experimental efforts to determine the behavior of individual devices in realistic circuits.

ACKNOWLEDGMENTS

We appreciate the support for this work provided by the Defense Threat Reduction Agency (DTRA) and the Army Research Office (ARO).

[1] W. Hu, H. Nakashima, K. Furukawa, Y. Kashimura, K. Ajito, Y. Liu, D. Zhu, and K. Torimitsu, J. Am. Chem. Soc. **127**, 2804 (2005).
[2] A. Dei, D. Gatteschi, C. Sangregorio, and L. Sorace, Acc. Chem. Res. **37**, 827 (2004).
[3] J. M. Seminario, P. A. Derosa, and J. L. Bastos, J. Am. Chem. Soc. **124**, 10266 (2002).
[4] J. M. Seminario, A. G. Zacarias, and J. M. Tour, J. Am. Chem. Soc. **122**, 3015 (2000).
[5] J. M. Seminario, A. G. Zacarias, and P. A. Derosa, J. Chem. Phys. **116**, 1671 (2002).
[6] X. H. Qiu, G. V. Nazin, and W. Ho, Phys. Rev. Lett. **93**, 196806 (2004).
[7] L. Cai, M. A. Cabassi, H. Yoon, O. M. Cabarcos, C. L. McGuiness, A. K. Flatt, D. L. Allara, J. M. Tour, and T. S. Mayer, Nano Lett. **5**, 2365 (2005).
[8] J. M. Seminario, L. E. Cordova, and P. A. Derosa, Proc. IEEE **91**, 1958 (2003).
[9] H. Basch and M. A. Ratner, J. Chem. Phys. **120**, 5761 (2004).
[10] B. Das and S. Abe, J. Phys. Chem. B **110**, 4247 (2006).
[11] W. Tian, S. Datta, S. Hong, R. Reifenberger, J. I. Henderson, and C. P. Kubiak, J. Chem. Phys. **109**, 2874 (1998).
[12] P. A. Derosa and J. M. Seminario, J. Phys. Chem. B **105**, 471 (2001).
[13] P. S. Damle, A. W. Ghosh, and S. Datta, Phys. Rev. B **64** 201403 (2001).
[14] M. Brandbyge, J. L. Mozos, P. Ordejon, J. Taylor, and K. Stokbro, Phys. Rev. B **65**, 165401 (2002).
[15] R. Landauer, IBM J. Res. Dev. **1**, 223 (1957).
[16] R. Landauer, Philos. Mag. **21**, 863 (1970).
[17] M. Buttiker, Y. Imry, R. Landauer, and S. Pinhas, Phys. Rev. B **31**, 6207 (1985).
[18] A. D. Becke, J. Chem. Phys. **98**, 5648 (1993).
[19] A. D. Becke, J. Chem. Phys. **98**, 1372 (1993).
[20] J. P. Perdew and Y. Wang, Phys. Rev. B **33**, 8800 (1986).
[21] J. P. Perdew and Y. Wang, Phys. Rev. B **45**, 13244 (1992).
[22] M. J. Frisch, G. W. Trucks, H. B. Schlegel, G. E. Scuseria, M. A. Robb, J. R. Cheeseman, J. A. Montgomery, T. Vreven Jr, K. N. Kudin, J. C. Burant, J. M. Millam, S. S. Iyengar, J. Tomasi, V. Barone, B. Mennucci, M. Cossi, G. Scalmani, N. Rega, G. A. Petersson, H. Nakatsuji, M. Hada, M. Ehara, K. Toyota, R. Fukuda, J. Hasegawa, M. Ishida, T. Nakajima, Y. Honda, O. Kitao, H. Nakai, M. Klene, X. Li, J. E. Knox, H. P. Hratchian, J. B. Cross, C. Adamo, J. Jaramillo, R. Gomperts, R. E. Stratmann, O. Yazyev, A. J. Austin, R. Cammi, C. Pomelli, J. W. Ochterski, P. Y. Ayala, K. Morokuma, G. A. Voth, P. Salvador, J. J. Dannenberg, V. G. Zakrzewski, S. Dapprich, A. D. Daniels, M. C. Strain, O. Farkas, D. K. Malick, A. D. Rabuck, K. Raghavachari, J. B. Foresman, J. V. Ortiz, Q. Cui, A. G. Baboul, S. Clifford, J. Cioslowski, B. B. Stefanov, G. Liu, A. Liashenko, P. Piskorz, I. Komaromi, R. L. Martin, D. J. Fox, T. Keith, M. A. Al-Laham, C. Y. Peng, A. Nanayakkara, M. Challacombe, P. M. W. Gill, B. Johnson, W. Chen, M. W. Wong, C. Gonzalez, and J. A. Pople, Gaussian 2003, Rev. B.4 (Gaussian, Inc., Pittsburgh PA, 2003).
[23] J. M. Seminario, L. Yan, and Y. Ma, Proc. IEEE **93**, 1753 (2005).
[24] C. Roetti, *in Quantum-Mechanical Ab initio Calculation of the properties of Crystalline Materials*, edited by C. Pisani (Springer-Verlag, Berlin, 1996), Vol. 67, p. 125.
[25] V. R. Saunders, R. Dovesi, C. Roetti, R. Orlando, C. M. Zicovich-Wilson, N. M. Harrison, K. Doll, B. Civalleri, I. Bush, P. D'Arco, and M. Llunell, *CRYSTAL2003 User's Manual* (University of Torino, Torino, 2003).
[26] P. A. M. Dirac, Proc. Cambridge Philos. Soc. **26**, 376 (1930).
[27] J. P. Perdew and A. Zunger, Phys. Rev. B **23**, 5048 (1981).
[28] P. J. Hay and W. R. Wadt, J. Chem. Phys. **82**, 270 (1985).
[29] W. R. Wadt and P. J. Hay, J. Chem. Phys. **82**, 284 (1985).
[30] P. J. Hay and W. R. Wadt, J. Chem. Phys. **82**, 299 (1985).
[31] D. R. Lide, *CRC Handbook of Chemistry and Physics* (CRC Press, Boca Raton, 1998), Vol. 79th Edition 1998–1999.
[32] J. M. Seminario and L. Yan, Int. J. Quantum Chem. **102**, 711 (2005).
[33] J. M. Seminario, C. E. De La Cruz, and P. A. Derosa, J. Am. Chem. Soc. **123**, 5616 (2001).
[34] J. M. Seminario, A. G. Zacarias, and P. A. Derosa, J. Phys. Chem. A **105**, 791 (2001).
[35] R. Dovesi, M. Causa, R. Orlando, C. Roetti, and V. R. Saunders, J. Chem. Phys. **92**, 7402 (1990).
[36] R. D. V. R. Saunders, C. Roetti, R. Orlando, C. M. Zicovich-

Wilson, K. D. N. M. Harrison, B. Civalleri, I. Bush, Ph. D'Arco, and M. Llunell, *CRYSTAL2003 User's Manual* (University of Torino, Torino, 2003).
[37] Z. Ning, J. Chen, S. Hou, J. Zhang, Z. Liang, J. Zhang, and R. Han, Phys. Rev. B **72**, 155403 (2005).
[38] C. K. Wang, Y. Fu, and Y. Luo, Phys. Chem. Chem. Phys. **3**, 5017 (2001).
[39] P. A. Derosa, V. Tarigopula, and J. M. Seminario, in *Encyclopedia of Nanoscience and Nanotechnology* (Dekker, New York, 2004).
[40] A. Troisi and M. A. Ratner, J. Am. Chem. Soc. **124**, 14528 (2002).
[41] P. A. Derosa, S. Guda, and J. M. Seminario, J. Am. Chem. Soc. **125**, 14240 (2003).
[42] J. M. Seminario, A. G. Zacarias, and J. M. Tour, J. Phys. Chem. A **103**, 7883 (1999).
[43] J. M. Seminario, R. A. Araujo, and L. Yan, J. Phys. Chem. B **108**, 6915 (2004).
[44] J. M. Seminario and P. A. Derosa, J. Am. Chem. Soc. **123**, 12418 (2001).
[45] P. Wang, C. N. Moorefield, S. Lic, S.-H. Hwang, C. D. Shreiner, and G. R. Newkome, Chem. Commun. (Cambridge) **10**, 1091 (2006).
[46] J. M. Seminario, C. De La Cruz, P. A. Derosa, and L. Yan, J. Phys. Chem. B **108**, 17879 (2004).
[47] J. J. Kushmerick, S. K. Pollack, J. C. Yang, J. Naciri, D. B. Holt, M. A. Ratner, and R. Shashidhar, Ann. N.Y. Acad. Sci. **1006**, 277 (2003).
[48] F. Evers, F. Weigend, and M. Koentopp, Phys. Rev. B **69**, 235411 (2004).
[49] A. Mackie and B. Warrick, Solid State Technol. **47**, 35 (2004).
[50] N. M. O'Boyle and J. G. Vos, GaussSum 1.0 (Dublin City University, 2005).
[51] T. T. Tsong, Phys. Rev. B **44**, 13703 (1991).
[52] F. Yin, R. Palmer, and Q. Guo, Phys. Rev. B **73**, 073405 (2006).